ELSEVIER

Atmospheric Research 85 (2007) 98–111

ATMOSPHERIC RESEARCH

www.elsevier.com/locate/atmos

Air quality assessment using a multi-instrument approach and air quality indexing in an urban area

E. Landulfo *, C.A. Matos, A.S. Torres, P. Sawamura, S.T. Uehara

IPEN – Instituto de Pesquisas Energéticas e Nucleares, Avenida Lineu Prestes 2242 – CEP 05508000, São Paulo – SP Brazil

Received 20 June 2006; accepted 19 November 2006

Abstract

An air quality monitoring methodology is presented here employing an elastic backscattering Lidar, sunphotometer data, air quality indexing and meteorological data in the city of São Paulo (23°33′ S, 46°44′ W), Brazil, a typical Urban Area. This procedure was made aiming to gather information from different optical atmospheric techniques and add this information to the air quality data provided regularly by the environmental agencies in the city. The parameters obtained by the Lidar system, such as planetary boundary layer height, aerosol optical thickness and aerosol extinction and backscattering aerosol coefficients are correlated with air quality indexes/reports provided by state environmental control agencies in order to extend the database information concerning pollution assessment and abate policies.

Keywords: Backscattering Lidar; Air quality; Planetary boundary layer; Aerosol

1. Introduction

Air pollution in megacities is one of the most important problems inherited from the 20th century. São Paulo is among the five largest metropolitan areas of the world, as well as one of the most populated with about 18 million inhabitants (Mage et al., 1996). In that instance human activities play an enormous impact on its air quality, as well as on their population health (Saldiva et al., 1995). The stress on environment due anthropogenic activities extends also to regional and global levels (Molina and Molina, 2004). Concerning the atmospheric quality there are many sources and types such as photochemical smog, ozone and its precursors and suspended aerosol particles. The latter is a subject of continuous interest due the on-going expansion of the São Paulo metropolitan area. The main aerosol sources include heavy industries, such as iron and steel works, refineries, chemical manufacturing, cement, sulphuric acid, petrochemical plants and the automotive fleet, in the case of the Metropolitan area of São Paulo (MASP) the vehicle fleet is already over 6 million units.

Regarding its topography the city of São Paulo is located in a plateau at about 800 m above sea level (ASL), and is surrounded by mountains of about 1200 m height. During the summer season the precipitation increases and many cold fronts generate meteorological instabilities, which indeed favor the pollution dispersion. These periods can extend over the autumn months of April, further on when the wintertime begins, a high-pressure semi-static regime over the São Paulo area is generally observed. This event becomes highly favorable to air

* Corresponding author. Fax: +55 11 38169315.
E-mail address: elandulf@ipen.br (E. Landulfo).

0169-8095/$ - see front matter © 2006 Elsevier B.V. All rights reserved.
doi:10.1016/j.atmosres.2006.11.008

pollutants accumulation, especially during episodes of intense temperature inversions (Castanho and Artaxo, 2001), occurring typically less than a 1000 m or even less than 200 m above the metropolitan area (Alonso and Romano, 1999).

In order to better address the air quality issue in São Paulo we employed a multi-instrument approach, ground-based sensors, namely a backscattering LIDAR (Light Detection and Ranging) system and a sunphotometer, and the data collected from radiosondes at a daily basis by the environmental agencies. The approach of using Lidars as an air quality assessment tool can provide in the long and short term a method of optimization for air pollution abatement strategies in need of new technologies to assess the air pollution problems (Calpini et al., 1997; Almbauer et al., 2000; Devara et al., 2002; Kambedizis et al., 1998; O'Neill et al., 2004; Kolev et al., 2004; Banta et al., 2005).

2. Experimental set-up and methodology

The LIDAR technique is based on the emission of a collimated laser beam in the atmosphere and on the detection of the backscattered laser light by the suspended atmospheric aerosols and atmospheric molecules. The LIDAR technique, through its high temporal (from seconds to minutes) and spatial (3–15 m) resolution is a powerful tool to visualize in real time, the structure of the Planetary Boundary Layer (PBL) using the aerosols as passive tracers of the atmospheric dynamic processes. A backscattering LIDAR can thus provide information on the PBL's mixed layer depth, entrainment zones and convective cells structure, aerosol distribution, clear air layering, cloud-top altitudes, cloud statistics, atmospheric transport processes and other inferences of air motion (Ferrare et al., 1991; Melfi et al., 1985; Crum et al., 1987; Balis et al., 2000).

A ground-based elastic backscatter Lidar system has been recently developed in the Laboratory of Environmental Laser Applications at the Centre for Laser and Applications (CLA) at the Instituto de Pesquisas Energéticas e Nucleares — IPEN. The Lidar system is a single-wavelength backscatter system pointing vertically to the zenith and operating in the coaxial mode.

The light source is based on a commercial Nd:YAG laser (Brilliant by Quantel SA) operating at the second harmonic frequency (SHF), namely at 532 nm, with a fixed repetition rate of 20 Hz. The average emitted power can be selected up to values as high as 3.3 W. The emitted laser pulses have a divergence of less than 0.5 mrad. A 30 cm diameter telescope (focal length $f = 1.3$ m) is used to collect the backscattered laser light. The telescope's field of view (FOV) is variable (0.5–5 mrad) by using a small diaphragm. The Lidar is currently used with a fixed FOV of the order of 1 mrad, which according to geometrical calculations (Chourdakis et al., 2002) permits a full overlap between the telescope FOV and the laser beam at heights around 300 m above the Lidar system. This FOV value, in accordance with the detection electronics, permits the probing of the atmosphere up to the free troposphere (5–6 km asl.).

The backscattered laser radiation is then sent to a photomultiplier tube (PMT) coupled to a narrow band (1 nm FWHM) interference filter, to assure the reduction of the solar background during daytime operation and to improve the signal-to-noise ration (SNR) at altitudes greater than 3 km. The PMT output signal is recorded by a Transient Recorder in both analog and photoncounting mode. Data are averaged between 2 and 5 min and then summed up over a period of about 1 h, with a typical spatial resolution of 15 m, which corresponds to a 100 ns temporal resolution.

Besides the Lidar measurements a co-located CIMEL aerosol measurements were performed to determine the AOT values at several wavelengths in the visible spectrum and thus to enable the assessment of the Aerosol Extinction values at the same spectral region. The principle of operation of the CIMEL instrument is to acquire aureole and sky radiances measurements. The standard measurements are taken 15 min apart, in order to allow for cloud contamination checking. These measurements are taken in the whole spectral interval, and their number depends on the daytime duration. The instrument precision and accuracy follow the standard Langley plot method within the standard employed by the AERONET network (Holben et al., 1998). The CIMEL sun photometer is calibrated periodically by a remote computer or locally under the supervision of the AERONET network. The calibration methodology assures coefficient accuracy between 1 and 3%, nonetheless various instrumental, calibration, atmospheric, and methodological factors influence the precision and accuracy, of optical thickness and effectively the total uncertainty in the AOT retrieved values is less than 8% (Chourdakis et al., 2002).

Radiosonde data were taken every day at 9 AM Local Time. The data allow establishing the structure of the atmosphere to about 4000 m in altitude and from them it is possible to achieve the main thermal inversion present at a given date and also compare its main features with those provided by the Lidar profiles.

The main environmental agency provides daily reports of a network of air quality stations scattered on the metropolitan area as showed in Fig. 1. It was also performed comparisons with the data of the pollution levels that were available and to establish a more representative average of the indices from 2 neighboring stations (at the sites Osasco and Pinheiros see Fig. 1 where the LIDAR site is also depicted — Ipen).

2.1. Lidar data retrieval

In the present stage, the retrieval of the aerosol optical properties is based on the measurements of the aerosol backscatter coefficient (βaer) at 532 nm, up to an altitude of 5–6 km The determination of the vertical profile of the aerosol backscatter coefficient relies on the LIDAR inversion technique following the Klett's

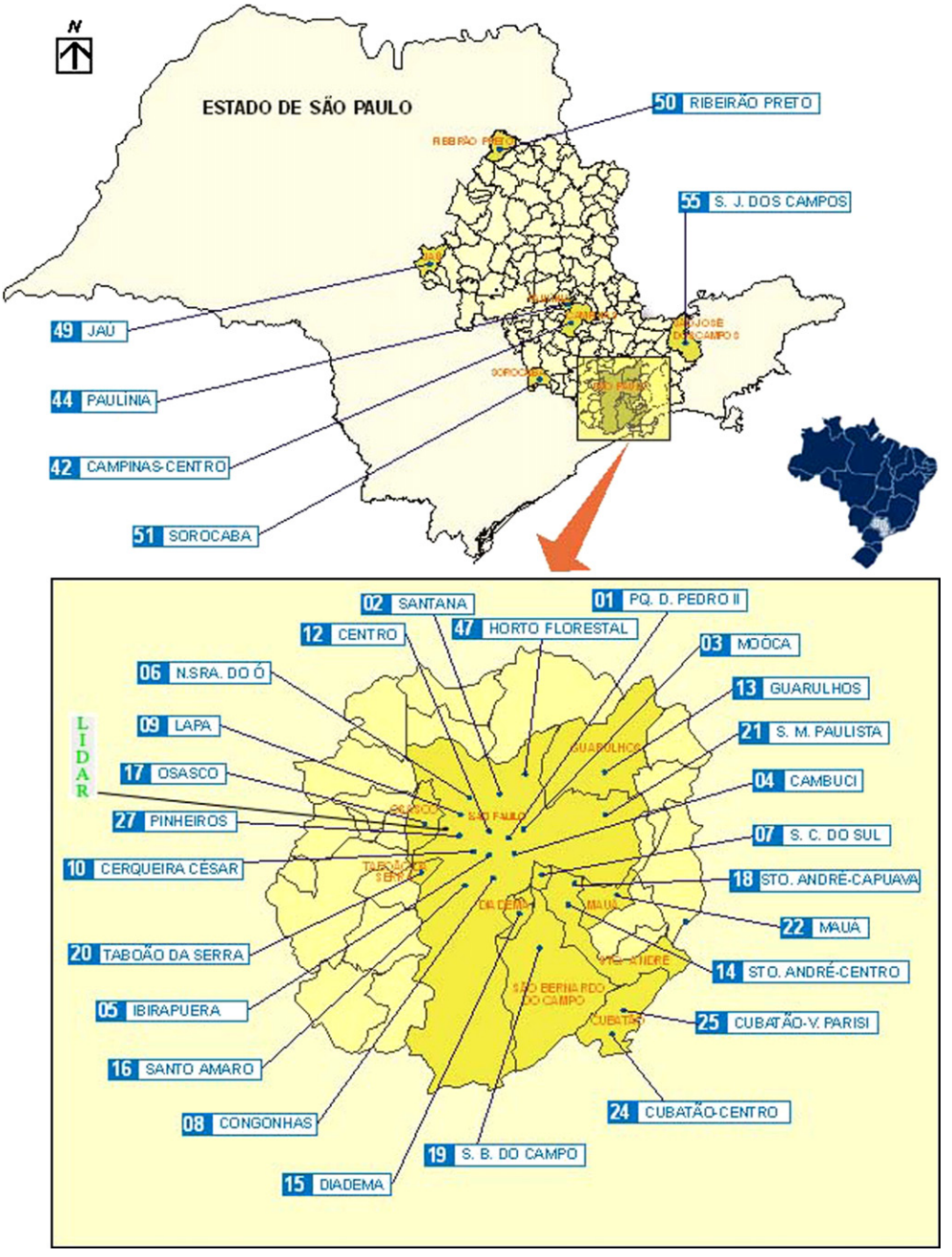

Fig. 1. Map of the CETESB air quality stations in the Sao Paulo State, adapted from the CETESB site.

algorithm, as proposed by Klett (Klett, 1985). In general, the inversion of the LIDAR profile is based on the solution of the LIDAR equation, under the assumption of the single scattering approximation:

$$P(\lambda,R) = PL\left(\frac{c\tau}{2}\right)\beta(\lambda,R)A_0\xi(\lambda)\zeta(R) \times R^{-2}\exp\left[-2\int_0^R \alpha(\lambda,r)dr\right] \quad (1)$$

where, $P(\lambda,R)$ is the LIDAR signal received from a distance R at the wavelength λ, PL is the emitted laser power, A_0 is the telescope receiving area, $\xi(\lambda)$ is the receiver's spectral transmission factor, $\beta(\lambda,R)$ is the atmospheric volume backscatter coefficient, $\zeta(R)$ is the overlap factor between the field of view of the telescope and the laser beam, $\alpha(\lambda,R)$ is the extinction coefficient, c is the light speed and τ is the laser pulse length.

In this equation, the α and β coefficients can be separated in two sets, one for the molecular scattering component and the other for the particle scattering component. Besides, in the Klett inversion technique, there is a reference altitude, Zref, used as an upper limit, and has to be an aerosol-free region. Therefore, in this region and above it, the LIDAR signal shows a decay, which follows the molecular contribution only.

One other straightforward data retrieval is the height from the Boundary-Layer (BL). Since this system monitors the various aerosol layer (AL) altitudes, one can assume that those higher altitude aerosol layer altitude correspond, within a margin of confidence, to the BL altitude (Coulter, 1979; De Wekker et al., 2002). Lidar data could be very useful for determining the BL altitude which is an important information in investigating pollution dispersion (Zilitinkevich and Baklanov, 2002) and prediction of air pollution enhancement episodes (El-Shahawy, 2002). Depending on how good and accurate is the Lidar data display one can within 10 – 30% error estimate the aerosol layers visually, one more accurate method is to take the first derivative of Lidar range-corrected signal:

$$S_{\text{corrected}} = (S_{\text{raw}} - \text{BG}) \times r^2 \quad (2)$$

$$\text{PBL}_{\text{height}} = \frac{d\ln(S_{\text{corr}}(r))}{dr} \quad (3)$$

where S_{raw} is the raw signal from the system in arbitrary units, BG is the background which can be inferred from an altitude where one assumes there is no aerosol contribution, usually 5–10 km, bearing in mind that due the occurrence of cirrus clouds this altitude would have to be shifted accordingly to avoid background contamination.

Following the method described above one can expect an overall uncertainty in the PBL and Mixed layer height retrieval of about 3 – 6% while the backscattering coefficients uncertainties are between 10 and 20% on the inversion method.

Attention should be given also to the fact there is a possibility of the mixing height being overestimated due pollutants trapped within the stable capping inversion (McElroy and Smith, 1991; Seibert et al., 2000).

There are cases when the data from the aerosol backscattering coefficients also provide information about the dust layers.

2.2. Sunphotometer data retrieval

The inversion of the solar radiances measured by the CIMEL sunphotometer to retrieve the aerosol optical thickness values (Holben et al., 1998), is based on the Beer–Lambert Eq. (4), assuming that the contribution of multiple scattering within the small field of view of the sunphotometer is negligible:

$$I_\lambda = I_\lambda^0 \exp\left(-\frac{\tau_\lambda}{\mu_S}\right) \quad (4)$$

where, I_λ and I_λ^0 are the solar irradiances at the top of the atmosphere and at ground level, respectively, and μ_S is the cosine of the solar zenith angle. τ_λ is the total atmospheric optical thickness from the Rayleigh and aerosol contributions, as well the ozone and water vapour absorption at 670 nm and 870 nm, respectively. The molecular (Rayleigh) scattering contribution is taken into account to retrieve the aerosol optical thickness values at 532 nm, determined by the relation:

$$\frac{\tau_{532}^{\text{aer}}}{\tau_{500}^{\text{aer}}} = \left(\frac{532}{500}\right)^{-\overset{0}{a}} \quad (5)$$

where, the Ångström exponent (Angström, 1964) $\mathring{a}$ was derived from the measured optical thickness in the blue and red channels (440 nm and 670 nm):

$$\overset{0}{a} = -\frac{\log\left(\tau_{440}^{\text{aer}}/\tau_{670}^{\text{aer}}\right)}{\log(440/670)} \quad (6)$$

Generally, the angstrom exponent provides information on the aerosol size distributions, with values greater than 2.0 corresponding to accumulation mode particles such as fresh biomass burning smoke and values closer to zero for coarse mode particles such as dust.

The CIMEL sun photometer is calibrated periodically by a remote computer or locally under the supervision of the AERONET network (Dubovik et al., 2000). The calibration methodology assures coefficient accuracy between 1 and 3%, nonetheless various instrumental, calibration, atmospheric, and methodological factors influence the precision and accuracy of optical thickness and effectively the total uncertainty in the AOT retrieved values is less than 8% (Balis et al., 2000).

2.3. Air quality data from the control environmental agency

The Air Quality Management Agency, namely CETESB (Company of Technology of Environmental Sanitation) has 29 air quality stations, 23 of these in the Metropolitan Area of Sao Paulo. This network provides the air quality data report (CETESB, 2005) based on a 24-hour average available daily. These daily air quality reports take into account the following pollutants: sulphur dioxide, inhalable particulate (PM 10), carbon monoxide, ozone and nitrogen dioxide. The index is obtained by a segmented linear function where the inflexion points are the air quality standards. Also from this function each pollutant is attributed an adimensional number referred to a scale. For report presentation purposes the highest index among the pollutants is presented. If the pollution index average is between 0 and 50, the condition of the air quality is considered good (G), when it is between 51 and 100 is considered fair (F), and when between 101 and 200, inadequate (I).

The equipment employed for these pollutants are based on automatic air quality stations which use equivalent methods certified by the United States Environmental Protection Agency (USEPA). The particulate material operates based on a beta absorption system, which is certified and calibrated every 3 months. The gas monitoring system is periodically calibrated every 3 months and has a daily check for baseline and linearity. Overall the values of concentration present an uncertainty between 1 and 2%, and the Air Quality Index has an uncertainty of about 4–5%. The data is generated every 5 s in the station network scattered over the MASP and by software an hourly average is provided and sent a central server where the data is checked for consistency — for each pollutant the related air quality index is published accordingly to the worst occurrence in the day, for ozone, the worst values in the last 4 h for nitrous dioxide, an 8 h average for the carbon monoxide and daily average for sulphur dioxide and inhalable particulate.

For the purpose of dispersion analysis the criteria applied are based on the inversion height from the radiosounding data, and by a calm wind index given in percentage which is extracted from a 24-h average of the wind speed from all stations in the network which are below 0.5 m/s, when these percentages are above 25% the day is considered unfavored for dispersion and favored for values below.

2.4. Radiosounding pbl height retrieval

The radiosounding measurements are take in a daily regime at 9 AM and 9 PM local time. The site is about 10 km from the Lidar site.

Different techniques can be used to obtain the PBL height from radiosoundings (De Tomasi and Perrone, 2006). For having a full scope of the PBL height one would need the bulk Richardson number, which implies the acquisition of the wind profile (Cooper and Eichinger, 1994). However these measurements would be worth if taken at the same site as the Lidar since the wind field can change dramatically even in a small scale.

Recently De Tomasi and Perrone showed three methods for extracting the PBL height. From those methods we apply here the critical inversion of the potential temperature and the method of inflexion points.

Accordingly we have the height in which a potential temperature critical inversion occurs applying three criteria:

The lapse rate (M1),

$$\frac{\Delta\theta}{\Delta z} > 0.005\ K/m \tag{7}$$

and a change in the potential temperature of:

$$\Delta\theta > 2K \tag{8}$$

where θ is the potential temperature and z is the altitude.

The other method (M2) for not only identifying the PBL heights but also aerosol layers is take the derivative of the potential temperature with respect to z and get the first and second maximum values.

In this present study we took a variant of the method above taking not only the first two inflexion points but others above, since it will be seen the radiosonde ratio started at about 700 m. Besides instead of taking a middle point in between the two consecutive points in an inflexion we took instead the leading point, e.g., the first point.

A third criterion (M3) would take the potential temperature which is equal to the one at ground level.

The uncertainties in the above methods are based on the retrieval of the temperature and pressure which are then used for evaluating the potential temperature.

Table 1
Meteorological data (temperature, relative humidity and atmospheric pressure at ground level) and dust layer and thermal heights for the selected days

Day	Time UTC	AQI	Ti – Tf °C	Pi –Pf mb	Ri–Rf %	DL(m)	TL(m)	F/U CW % Ws (m/s)
3/23/2004	21:25–21:55	G(33)	17.7 – 17.4	928.9 – 928.9	76 – 77	640, 1480	679, 1533, 548	F 12.9 1.9
4/12/2004	12:42–13:09	G(44)	23.9 – 24.6	926.0 – 926.0	67 – 65	526, 1980	544, 606, 2002	F 13.9 1.7
4/30/2004	14:05–14:11	F(56)	21.4 – 21.6	928.6 – 927.9	53 – 47	265, 1340	288, 340, 1375	F 9.8 1.5
8/9/2004	12:45–13:15	G(32)	11.9 – 13.6	937.7 – 937.4	67 – 59	685	394, 612, 2155	F 8.8 2.1
8/19/2004	12:49–13:19	I(111)	20.5 – 21.5	933.3 – 933.1	58 – 53	544, 950, 1480	186, 250, 1453	U 43.1 1.3
8/20/2004	12:14–12:44	F(86)	19.1 – 20.7	931.9 – 931.8	69 – 60	435, 1100	250, 1254	U 34.3 1.5
9/9/2004	12:26–12:56	F(96)	22.4 – 23.3	928.0 – 928.0	42 – 40	366, 1530	180, 268, 1688	U 37.5 1.4
9/10/2004	12:50–13:20	I(106)	22.2 – 22.8	929.1 – 928.8	60 – 55	485, 1002, 2200	355, 425, 2116	F 16.2 1.6

In the last column it is given the dispersion classification U (unfavorable), F (favorable) based in the calm wind speed percentage and the 24 h average of the wind speed at surface — one should bear in mind that for this average the values below 0.5 m/s are not taken into account.

The temperatures and pressure have an uncertainty less than 1% and following the appropriate error propagation the potential temperatures will have roughly 0.5–0.8% errors. Those errors though are statistical and above methods for taking the inversion layers are in general subject to systematic error rather than statistical ones which might at first approach enhance the overall uncertainty to a few percent, however the exact values should be better evaluated in a future work.

3. Results and discussion

To give a broad overview we took some sample days chosen in the year of 2004, in which different air quality and meteorological conditions were present. Mainly we have an intercomparison of the dust layers and thermal layers with the Lidar and radiosonde data, respectively. The optical properties for aerosols are then investigated through the analysis of the Aerosol Optical Thickness (AOT) and Angstrom exponent retrieved from the sunphotometer and then further analyzed by the aerosol backscattering coefficients extracted from the Lidar data. Besides we provide some meteorological data as temperature, pressure and relative humidity during the period of measurements. The meteorological conditions of the selected days are given in Table 1. In Table one we have available the values for the Dust Layers (DL) retrieved with the Lidar system and the Thermal Layers (TL) given by the Radiosounding (RS) data, and the dispersion classification U (unfavorable), F (favorable) based in the calm wind speed percentage and the 24 h average of the wind speed at surface.

3.1. Day 03/23/2004

On the 23rd of March, the meteorological conditions are given in Table 1, the previous days there was some precipitation that "cleaned" the atmosphere, which indicates a good condition for dispersion as seen from the last column from the dispersion conditions (calm wind index (CWI)=12.9%). This is reflected by the good air quality index, 33. From the Lidar×radiosonde plots, Fig. 2a, it can be seen the thermal layers at 679 m (M1), 1533 m (M2) and 548 m (M3) for the radiosonde and for the Lidar the dust layers are at 640 m and also a mixing layer between 700 m and 1650 m for the Lidar representing a dust layer and temperature layer up to 1533 m for the RS. From previous works (Cooper and Eichinger, 1994) one can interpret the layers as the entrainment zone (1400 – 2500 m) and a Mixing Layer below 700 – 1400 m as seen in the aerosol backscattering coefficient profiles, (Fig. 4a). The discrepancy in the altitudes between the Lidar and radiosonde could have to do with the difference in time between the measurements, the different site locations and the fact the radiosonde data is taken every 15 min and in one ascendant flight while the Lidar data is an average of every 3–5 min. The sunphotometer data show a very low AOT for the period of the measurement indicating a low aerosol load in the atmosphere, the AE is around 1.15 (Fig. 2a) suggesting the presence of larger particles and a stable value during the measurement implies no significant change in the aerosol load. When one looks at the retrieved aerosol backscattering coefficients profiles (Fig. 4a), it can be noted a very small absolute values for the backscattering, around 10^{-4} km^{-1} sr^{-1}, once again endorsing the good air quality for this day.

3.2. Day 04/12/2004

This day is considered also good for air quality purposes, as the AQI is equal to 44, nonetheless very near in value to a fair day (AQI greater than 50). The ground meteorological data in Table 1 show a slightly

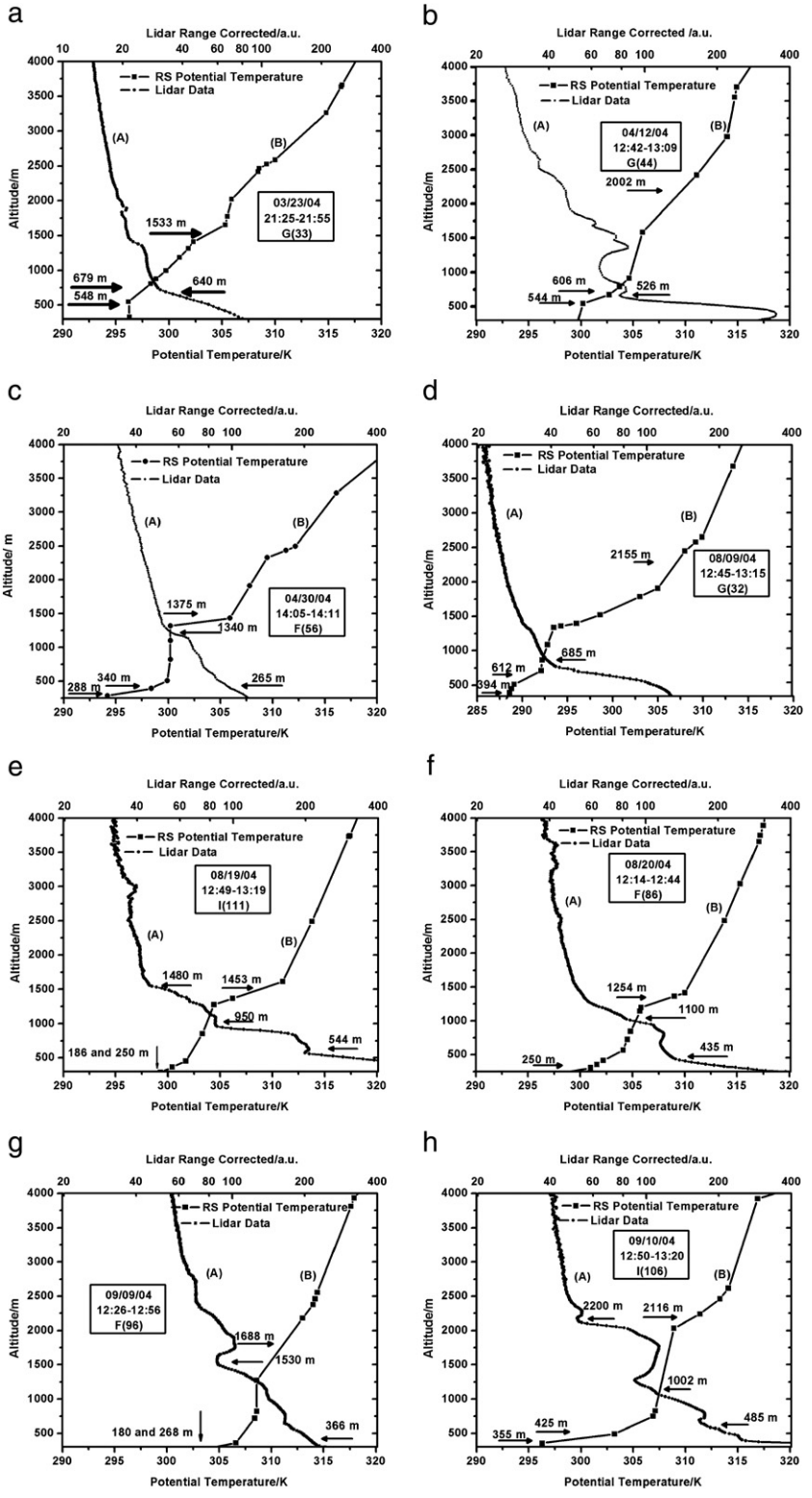
a
Lidar Range Corrected/a.u.
RS Potential Temperature
Lidar Data
(A)
(B)
03/23/04
21:25-21:55
G(33)
1533 m
679 m
548 m
640 m
Altitude/m
Potential Temperature/K
b
Lidar Range Corrected /a.u.
RS Potential Temperature
Lidar Data
(A)
(B)
04/12/04
12:42-13:09
G(44)
2002 m
606 m
544 m
526 m
Altitude/m
Potential Temperature/K
c
Lidar Range Corrected/a.u.
RS Potential Temperature
Lidar Data
(A)
(B)
04/30/04
14:05-14:11
F(56)
1375 m
1340 m
340 m
288 m
265 m
Altitude/ m
Potential Temperature/K
d
Lidar Range Corrected/a.u.
RS Potential Temperature
Lidar Data
(A)
(B)
08/09/04
12:45-13:15
G(32)
2155 m
685 m
612 m
394 m
Altitude/m
Potential Temperature/K
e
Lidar Range Corrected/a.u.
RS Potential Temperature
Lidar Data
08/19/04
12:49-13:19
I(111)
(A)
(B)
1480 m
1453 m
950 m
544 m
186 and 250 m
Altitude/m
Potential Temperature/K
f
Lidar Range Corrected/a.u.
RS Potential Temperature
Lidar Data
08/20/04
12:14-12:44
F(86)
(A)
(B)
1254 m
1100 m
435 m
250 m
Altitude/m
Potential Temperature/K
g
Lidar Range Corrected/a.u.
RS Potential Temperature
Lidar Data
09/09/04
12:26-12:56
F(96)
(A)
(B)
1688 m
1530 m
180 and 268 m
366 m
Altitude/m
Potential Temperature/K
h
Lidar Range Corrected/a.u.
RS Potential Temperature
Lidar Data
09/10/04
12:50-13:20
I(106)
(A)
(B)
2200 m
2116 m
1002 m
425 m
355 m
485 m
Altitude/m
Potential Temperature/K

increase in temperature followed by an also small decrease in the relative humidity, while the dispersion conditions are good given the CWI of 13.9% and an average wind of 1.7 m/s. One can observe a layered structure in the Lidar profile (Fig. 2b) which is less evident in the RS data, which is due the transport of aerosols by the wind at higher altitudes during the measurement, thus increasing the number of dust layers and thin clouds. The presence of three thermal layers, again in Fig. 2b, one at 544 m (M3), other at 606 m (M1) and other at 2002 m (M2) strongly suggests an uplift of air bringing up aerosols which contribute to a cleansing in the air near the surface and, therefore, improving the air quality. The number of dust layers from the Lidar data (the lowest) at 526 m also indicates the uplifting of air cleaning the aerosols from near the surface and one can see a Residual Layer from the previous days above up to 2600 m as also seen in the aerosol backscattering coefficient profile, (Fig. 4b).

The AOT-AE plot for this day in (Fig. 3b) shows a moderate to high values for the aerosol thickness and highly varying values through the period of the measurement, 0.27 to 0.40, which brings the fact that due the existing winds a lot of transport might have taken place, the Angström exponent evolution shows also some changes which are not so drastic, but one can see that the higher values of AE (1.36) correspond to lower values of AOT, while the values at around 1.28 correspond to higher values in the AOT.

The absolute values for the aerosol backscattering coefficients are one order of magnitude higher than those given for 03/23, around 10^{-3} km^{-1} sr^{-1}, indicating the presence of scattering particles, not only close to the ground but also in the region between 900 and 2500 m.

3.3. Day 04/30/2004

This day, considered fair and with an AQI of 56 shows meteorological conditions not as favorable since it is relatively dry with an average RH of 50%. The CWI is about 9.8% and the average wind 1.5 m/s, both indicating favorable conditions, which might be in contradiction with the fair conditions for the air quality, one has however to bear in mind that the favorable conditions are taken considering the whole Sao Paulo Metropolitan area while the AQI is more localized, besides there might be that for these days the impact of aerosols in the air quality are less significant as for other pollutants. The layers shown in Fig. 2c by the RS data reveal thermal layers at 288 m (M3), 340 m (M1) and 1375 m (M2), in the latter a constant potential temperature occurs indicating poor dispersion conditions. The dust layers extracted from the Lidar Data are located at 265 m and 1340 m. The aerosol backscattering coefficients profile in Fig. 4c also indicates a ML at 1440 m, and a very high value for the end of the PBL (4000 m). This could be due a jet bringing up aerosols, even in small amounts, into the free atmosphere and avoiding a more accurate and precise measurement during the aforementioned period. By inspecting the behavior of the AOT – AE plots one observes in both quantities an abrupt change at 11:20 LT (14:20 UTC) when a sudden drop in the AOT occurs followed by a change in the AE as well, the change in this values gives the idea of a depletion of aerosols once again suggesting the occurrence of an air jet or the breaking of the entrainment zone (Stull, 1991). The backscattering coefficient profile in Fig. 4c indicates the same behavior as in the Lidar signal plot and shows a mixing layer between 800 m and 1600 m. This difference has to deal with the fact that the range corrected Lidar signal carries the molecular signal with it while the backscattering profile is a pure aerosol signature enhancing the usefulness of these plots, however due the inversion method employed some smoothing occurs which could be less sensitive to subtle changes in the atmosphere layering structure.

3.4. Day 08/09/2004

This day shows the best (lowest) air quality (AQI = 32) among those selected and resembles a lot like day 1 exemplifying a potential signature in the Lidar profile for this kind of days (Landulfo et al., 2003). The meteorological and dispersion conditions are by far the best among the values given in Table 1 endorsing a very good relation among these parameters. Since this period of the year corresponds to the winter (dry season) we observe a low temperature but not a so dry atmosphere near the ground (RH spans from 68 to 57%). The thermal layers shown in Fig. 2d are present at 394 m (M3), 612 m (M1) and 2155 m (M2) while there is only a dust layer at 685 m. It is important here to observe that

Fig. 2. Radiosounding (A) and Lidar data (B) for the selected days in 2004: 03/23 a); 04/12 b); 04/30 c); 08/09 d); 08/19 e); 08/20 f); 09/09 g) and 09/10 h). For the sake of comparison we have in each panel information about the Air Quality Index (AQI) available from the local air quality management agency, also in those panels one can see the indication with arrows of Dust Layers (DL) in the Lidar profiles and Thermal Layers (TL) for the radiosounding profiles. The methods for identifying those layers are given in sections Lidar Data and pbl Height Retrieval.

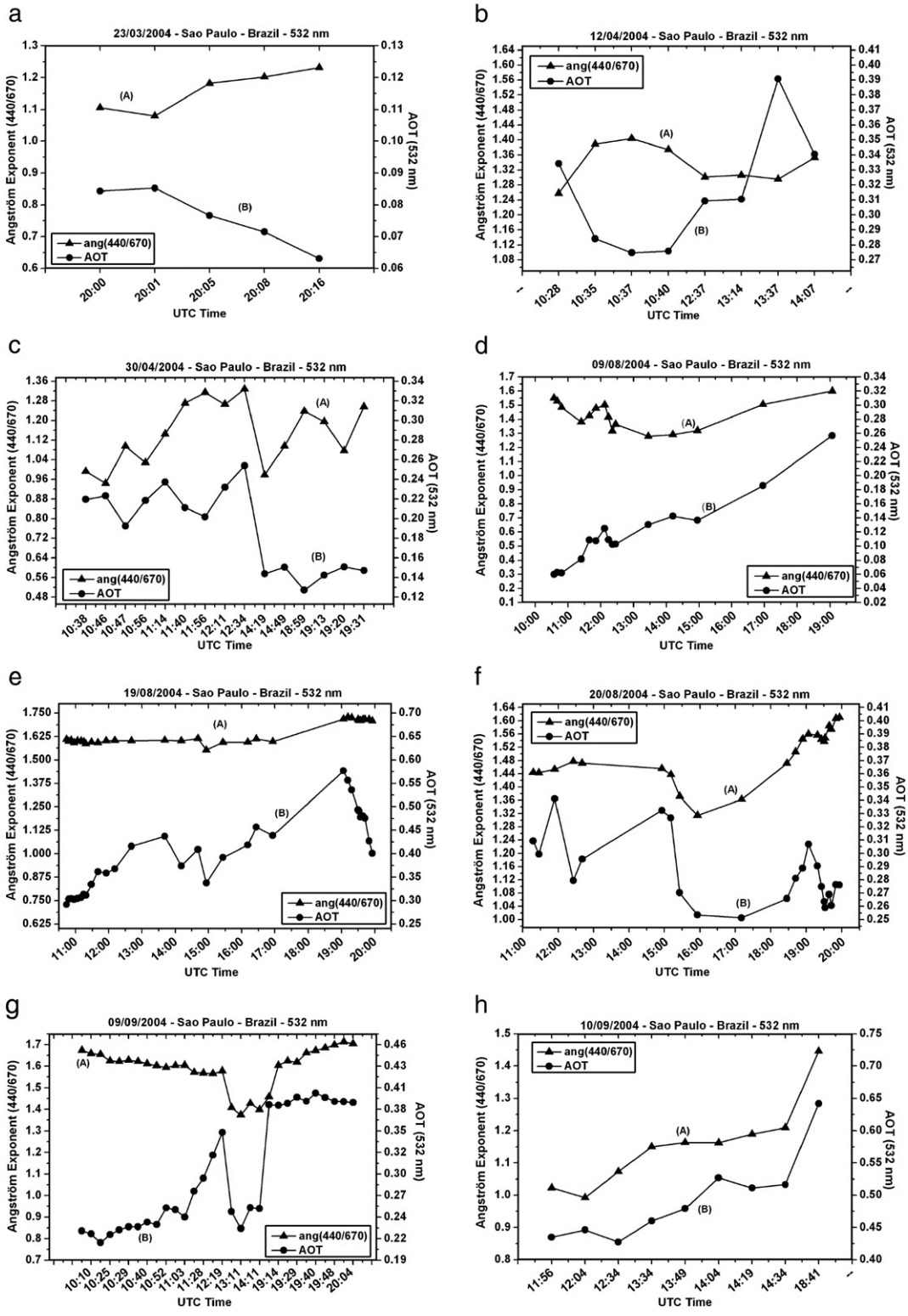

Fig. 3. Ångström Exponent — AE (A) and Aerosol Optical Thickness — AOT (B) at 532 nm for the selected days: in 2004: 03/23 a); 04/12 b); 04/30 c); 08/09 d); 08/19 e); 08/20 f); 09/09 g) and 09/10 h). These quantities are obtained from the sunphotometer belonging to the Aeronet (Holben et al., 1998) and are used for the average size distribution (AE) and for the tuning of the Lidar retrieval (AOT), Landulfo et al. (2003).

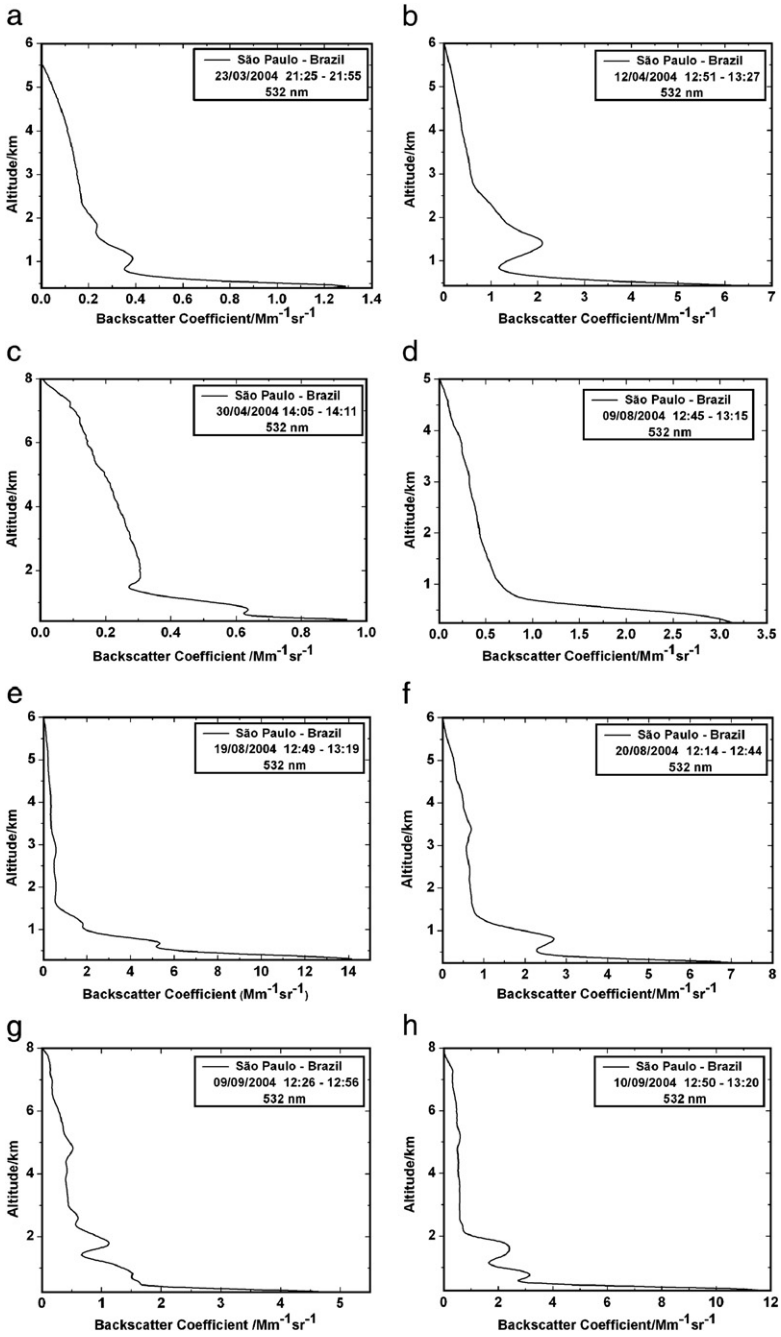

Fig. 4. Aerosol Backscattering Coefficient at 532 nm for the selected days: in 2004: 03/23 a); 04/12 b); 04/30 c); 08/09 d); 08/19 e); 08/20 f); 09/09 g) and 09/10 h). These plots were obtained through the analysis of the Lidar signal following the method described in section Lidar data retrieval (Klett, 1985). The aerosol backscattering coefficient provides an alternative way o visualizing the Dust layers present in the atmosphere, where the scattering signal from the molecules are extracted, one has to bear in mind though there are some degree of smoothing which might eliminate finer structures present in the aerosol profiles.

some authors (Cooper and Eichinger, 1994) would have a different interpretation of the data herein showed and attributing the PBL height up to 2500 m and dividing the mixing layer into two sub-layers: a convective one formed under unstable conditions and a mechanical one formed by the action of wind shear, jets and low frequency bursts. This very detailed description is more meaningful when the wind field is also provided and for

the sake of the simplicity of our methodology is still significant in comparing those results. The AOT – AE plots (Fig. 3d) show for the period of the measurement a low value of AOT, namely 0.14 as one can see in this day a steady increase of its value. The AE for the period is of 1.5 indicating smaller particles present in the atmosphere in opposition to those values on the 23rd of March. The backscattering profile (Fig. 4d) shows an inversion around 1000 m and very low absolute values, 0.0030 km^{-1} sr^{-1} which corroborates the low presence of particles and a correspondent good air quality.

3.5. Day 08/19/2004

This day is an example of a highly polluted day (AQI=111) much more common during this period of the year due the poor dispersion conditions as seen from Table 1. The meteorological data at the ground show an average mean RH of 55. Again we observe an increase/decrease in temperature/relative humidity during the period of the measurement. The thermal layers in Fig. 2e by methods M3 and M1 are at a very low altitude, 250 m and 186 m, while by method M2 one can see other at 1453 m. The dust layers are located at 544 m, 950 m and at 1489 m very close to the M2 thermal layer. The intensity of the range corrected Lidar signal is comparatively very high being an indication of a high load of aerosols near the surface responsible indeed for the very poor air quality.

The AOT–AE plots in Fig. 3e show high values of AOT during the measurement, around 0.40 and peaking up to 0.60 in this day. The AE is around 1.60 corresponding to fine particles.

The backscattering coefficient profile in Fig. 4e gives absolute high values, 0.014 km^{-1} sr^{-1}, which is 20 times higher than in a good air quality day and the presence of the two layers as in the case of the Lidar/RS plots.

3.6. Day 08/20/2004

This is a fair air quality index day (86) suggesting a better dispersion condition than the previous day. The relative humidity had a mean value of 65 and a temperature typical for this period of the year, we verify again an increase/decrease feature in the temperature/RU behavior and the dispersion conditions are unfavorable, which keeps the AQI in such a high value despite being considered fair. The number of thermal layers in Fig. 2f are reduced to 2 since the M2 method could not be fulfilled thus one can find a thermal layer at 250 m (M3) and at 1254 m (M2). Two dust layers were identified at 435 m and at 1100 m. The AOT and AE plots in Fig. 3f for this day present a interesting feature as one observe that up to the time of the measurement the value was relatively high (0.32) and has a sudden drop also accompanied by a significant change in the AE suggesting a change on type (optical properties) of aerosol. This behavior has to do with the dispersion of the pollutants as the mixing layer breaks and favors a mixing of the lower air parcels (more polluted) with the upper ones. The backscattering coefficient profile presents the mixing layer between 500 and 1000 m (Fig. 4f). It is noteworthy to mention that the measurement was taken during a condition in which the lower atmosphere was more loaded with aerosols.

3.7. Day 09/09/2004

Presenting an AQI of 96, which is relatively high, this day, is considered a fair air quality day according to the scale presented however the Lidar profile Fig. 2g shows some features of a polluted day like a large Lidar Range Corrected signal. The RH spans between 40 and 42%, the lowest of days chosen and an average temperature of 22 °C, the dispersion conditions are poor as seen from Table 1 (CWI=34.5% and wind speed=1.5 m/s). There is a minor decrease in the RH followed by a raise in temperature. Like day 08/19/04 there are very low M3 and M1 thermal layers at 180 m and 268 m and another one at 1688 m (M2), Fig. 2g. The presence of dust layers was taken at 366 m and at 1530 m. It is interesting to observe in the Lidar profile a rather higher layer between 1500 m and 2000 m. The AOT and AE plots in Fig. 3g show for the period of measurement a sudden drop in value which is again an indicative of cleansing in the atmosphere due winds and possible PBL break down (Mahrt, 1999). In this process the changes in the AE is an indicative of a difference in the optical properties of the atmosphere. The backscattering coefficient profile enhances the presence of the higher aerosol layer and a lower inversion around 1300 m, Fig. 4g.

3.8. Day 10/09/2004

The second worst day concerning the air quality (AQI=109), this day is relatively wetter than the previous day (09/09) and with a similar average temperature (around 22.5 °C), also from Table 1. We see that the dispersion conditions are favored which might due the fact the worst air quality conditions were still in place at the time the measurement was taken while the daily conditions for dispersion got better throughout the

day. The thermal layers are at 355 m (M3), 425 m (M1) and 2116 m (M2) while the dust layers are at 485 m, 1002 m and 2200 m in Fig. 2h, the latter suggests that an aerosol load cold have been transported rather than have been originated locally. The higher aerosol layer is much more pronounced indicating a poor dispersion in the 24 period. The RS profile structure shows an almost constant potential temperature between 1000 m and 2500 m given more ground to the idea of a poor quality dispersion condition for this given day. The AOT plot in Fig. 3h shows higher values for the AOT peaking at almost 0.75, and an average value for AE of 1.1 suggesting a larger type of aerosols. The backscattering coefficient profile in Fig. 4h shows also a multi-layered structure of the atmosphere up to 2000 m. It is worth to mention that those profiles with multi-layered structure are in general related to a poor quality day while those with less layering are more prone to be a good air quality day.

For the purpose of some statistical analysis we made a plot in Fig. 5 of Aerosol Optical Thickness provided by the sunphotometer/Lidar measurements *versus* the Air Quality Index from the fixed stations and the correlation obtained is very high ~ 0.85 which can be noticed easily in the plot for the majority of the days takes as case studies, one exception however can be seen for 04/12, a fair day with an unusual high AOT, this may be due a transport which did not affected locally the MASP.

Another analysis is to verify some correlation between the Lidar layering structure which can in a first approach be quantified with the altitude of the highest layer in the Lidar data, from Fig. 6 one sees that the worst the air quality gets (high AQI) the highest the highest layer is, in addition if the RS data are taken into account an inverse behavior is observed, i.e. the height of the lowest RS layer gets lower as the AQI gets poorer. These empirical approaches have to be better studied in a boundary layer modeling context and with an increased number of case studies to fully enhance our analysis.

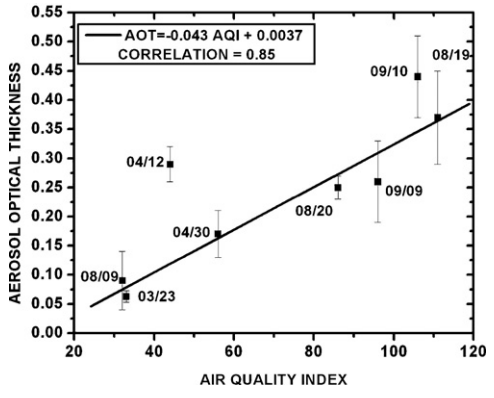

Fig. 5. A plot of the correlation between the Aerosol Optical Thickness and the Air Quality Index from the days in study. The correlation factor is about 0.85 indicating a strong correlation among the data.

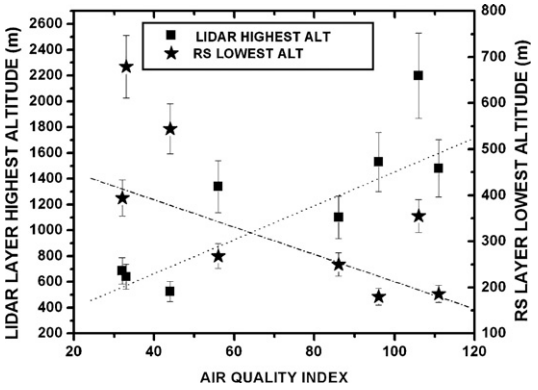

Fig. 6. The behavior of the observed heights for the Highest Lidar Layer Altitude (squares) showing an increase with poorer air quality conditions. An inverse trend is observed if the Lowest RS Layer Altitude (stars) is observed, as the layers are lowers as the air quality gets worse.

4. Conclusions

An intercomparison of the dust layers and thermal layers with the Lidar and radiosonde data was conducted as well the optical properties for aerosols were then investigated through the analysis of the Aerosol Optical Thickness (AOT) and Angstrom exponent retrieved from a AERONET sunphotometer. By identifying the dust layers (LIDAR) and thermal layers (RS) it was realized that the worse the condition in air quality the more stratified the atmosphere was, enhancing the idea of poor dispersion conditions in this kind of days. It is noteworthy to mention that from the different methods of giving a thermal layer the correspondence with the Lidar dust layer presence was not matching precisely for reasons like: different locations, different time frame and resolution between the radiosounding procedure and Lidar data acquisition. One other interesting point is that not always an inversion in thermal layer is detected by a Lidar system since there are not enough aerosols to provide enough signal.

From the aerosol backscattering coefficient profiles given by the Lidar analysis it was verified again that a multilayered structure was related to a poor air quality condition and from the absolute maximum values at the plots also there was a straightforward correspondence between high air quality indexes and high backscattering

coefficient values. The sunphotometer data provided an overall aerosol physical property extracted from the Angstrom exponent and aerosol optical thickness variation during the given days. We observed that during the time the measurement was taken mainly dictated by the radiossounding procedure that some sudden changes in the AOT′s and AE′s were observed due probably to the presence of jets induced by convection and mixing layer breakdown.

This effort was useful in putting together many instrumental resources to monitor the air quality together with the regular equipment and procedure employed by the city air quality agency and pinpoint the many details each instrument provide to characterize a good/bad air quality condition within an urban area like the city of São Paulo.

Acknowledgments

The authors would like to thank the funding agency for their research support namely Fundação de Amparo À Pesquisa do Estado de São Paulo, FAPESP (04/12583-1), Conselho Nacional de Desenvolvimento Científico e Tecnológico and Pesquisa and Coordenação de Aperfeiçoamento de Pessoal de Nível Superior. Also we would like to thank Dr. Paulo Artaxo for maintaining the AERONET database and Carlos Ibsen Lacava, Ricardo Anazia and Daniel Silveira Lopes from CETESB for providing the air quality data.

References

Almbauer, R.A., Oettl, D., Bacher, M., Sturm, P.J., 2000. Simulation of the air duality during a field study for the city of Graz. Atmos. Environ. 34 (27), 4581–4594.

Alonso, C.D., Romano, J., 1999. Metropolitan Area Air Quality Annual Report. Sao Paulo State Environmental Protection Agency.

Angström, A., 1964. The parameters of atmospheric turbidity. Tellus 16, 64–75.

Banta, R.M., Senff, C.J., Nielsen-Gammon, J., Darby, L.S., Ryerson, T.B., Alvarez, R.J., Sandberg, S.P., Williams, E.J., Trainer, M., 2005. A bad air day in Houston. Bull. Am. Meteorol. Soc. 657–669. doi:10.1175/BAMS-865-657.

Balis, D., Papayannis, A., Galani, E., Marenco, F., Santacesaria, V., Hamonou, E., Chazette, P., Ziomas, I., Zerefos, C., 2000. Tropospheric LIDAR aerosol measurements and sun photometric observations at Thessaloniki. Atmos. Environ. 34, 925–932.

Calpini, B., Simeonov, V., Jeanneret, F., Kuebler, J., Stahya, V., vandenBergh, H., 1997. Ozone LIDAR as an analytical tool in effective air pollution management: the Geneva 96 campaign. Chimia 51 (10), 700–704.

Castanho, A.D.A., Artaxo, P., 2001. Wintertime and summertime São Paulo aerosol source apportionment study. Atmos. Environ. 35, 4889–4902.

Relatório de qualidade do ar no estado de São Paulo/CETESB, 2005.

Chourdakis, G., Papayannis, A., Porteneuve, J., 2002. Analysis of the receiver response for a non-coaxial LIDAR system with fiber-optic output. Appl. Opt. 41, 2715–2723.

Cooper, D.I., Eichinger, W.E., 1994. Structure of the atmosphere in an urban planetary boundary layer from Lidar and radiosonde observations. J. Geophys. Res. 99 (D11), 22937–22948.

Coulter, R.L., 1979. Comparison of 3 methods for measuring mixing-layer height. J. Appl. Meteorol. 18 (11), 1495–1499.

Crum, T., Stull, R., Eloranta, E., 1987. Coincident Lidar and aircraft observations of entrainment into thermal and mixed layers. J. Clim. Appl. Meteorol. 26, 774–788.

De Tomasi, F., Perrone, M.R., 2006. PBL and dust layer seasonal evolution by Lidar and radiosounding measurements over a peninsular site. Atmos. Res. 80, 86–103.

Devara, P.C.S., Maheskumar, R.S., Raj, P.E., Pandithurai, G., Dani, K.K., 2002. Recent trends in aerosol climatology and air pollution as inferred from multi-year Lidar observations over a Tropical Urban Station. Int. J. Climatol. 22, 435–449.

De Wekker, S.F.J., Steyn, D.G., Nyeky, S., 2004. A comparison of aerosol-layer and convective boundary-layer structure over a mountain range during Staaarte ’97. Boundary-Layer Meteorol. 113, 249–271.

Dubovik, O., Smirnov, A., Holben, B.N., King, M.D., Kaufman, Y.J., Eck, T.F., Slutsker, I., 2000. Accuracy assessments of aerosol optical properties retrieved from Aerosol Robotic Network (AERONET) Sun and sky radiance measurements. J. Geophys. Res. 105 (D8), 9791–9806.

El-Shahawy, M.A., 2002. Prediction of air-pollution episodes. Boundary-Layer Meteorol. 104, 319–329.

Ferrare, R.A., Schols, J.L., Eloranta, E.W., 1991. Lidar observations of banded convection during BLX83. J. Appl. Meteorol. 30, 312–326.

Holben, B.N., Eck, T.F., Slustker, I., Tanré, D., Buis, J.P., Setzer, A., Vermote, E., Reagan, J.A., Kaufman, Y.J., Nakajima, T., Lavenu, F., Jankowiak, I., Sminov, A., 1998. Aeronet — a federal instrument network and data archive for aerosol characterization. Remote Sens. Environ. 66, 1–16.

Kambezidis, H.D., Weidauer, D., Melas, D., Ulbricth, M., 1998. Air quality in the Athens Basin during sea breeze and non-sea breeze days using laser-remote sensing. Atmos. Environ. 32 (12), 2173–2182.

Klett, J., 1985. Lidar inversion with variable backscatter/extinction ratios. Appl. Opt. 24, 1638–1643.

Kolev, N., Tatatov, B., Kaprielov, B., Koley, I., 2004. Investigation of the aerosol structure over an urban area using a polarization Lidar. J. Environ. Monit. 6, 834–840.

Landulfo, E., Papayannis, A., Artaxo, P., Castanho, A.D.A., Freitas, A.Z., Souza, R.F., Vieria Junior, N.D., Jorge, M.P.M.P., Sánchez-CCoyllo, O.R., Moreira, D.S., 2003. Synergetic measurements of aerosols over São Paulo, Brazil using LIDAR, sunphotometer and satellite data during the dry season. Atmos. Chem. Phys. 3 (5), 1523–1539.

Mage, D., Ozolins, G., Peterson, P., Webster, A., Orthofer, R., Vanderweerd, V., Gwynne, M., 1996. Urban air pollution in megacities of the world. Atmospheric. Atmos. Environ. 30 (5), 681–686.

Mahrt, L., 1999. Stratified atmospheric boundary layers. Atmospheric boundary layers. Boundary-Layer Meteorol. 90, 375–396.

McElroy, J.L., Smith, T.B., 1991. Lidar descriptions of mixed layer thickness characteristics in a complex terrain/coastal environment. J. Appl. Meteorol. 30, 585–597.

Melfi, S.H., Spinhime, J., Chou, S.-C., Palm, S., 1985. Lidar observations of vertically organized convection in the planetary

boundary-layer over the ocean. J. Clim. Appl. Meteorol. 24, 806–821.

Molina, M.J., Molina, L.T., 2004. Urban Biosphere and Society: Part. Cities. Ann. N.Y. Acad. Sci. 1023, 142–158.

O'Neill, N.T., Strawbridge, K.B., Thulasirama, S., Zhang, J., Royer, A., Freemantle, J., 2004. Optical coherency of sunphotometry, sky radiometry and Lidar measurements during the early phase of Pacific 2001. Atmos. Environ. 38, 5887–5894.

Saldiva, P.H.N., Pope, C.A., Scharwtz, J., Dockery, D.W., Lichtnfels, A.J., Salge, J.M., Barone, I., Bohm, G.M., 1995. *Arch.* Air pollution and mortality in elderly people: a time-series study in São Paulo, Brazil. Environ. Health 50, 159–163.

Seibert, P., Beyrich, F., Gryning, S., Joffre, S., Rasmussen, A., Tercier, P., 2000. Review and intercomparison of operational methods for the determination of the mixing height. Atmos. Environ. 34, 1001–1027.

Stull, R.B., 1991. An Introduction to Boundary Layer Meteorology.

Zilitinkevich, S., Baklanov, A., 2002. Calculation of the height of the stable boundary layer in practical applications. Boundary-Layer Meteorol. 105, 389–409.